In Vivo Detection of Phospholipase C by Enzyme-Activated Near-Infrared Probes

ARTICLE *in* BIOCONJUGATE CHEMISTRY · DECEMBER 2011

Impact Factor: 4.51 · DOI: 10.1021/bc200242v · Source: PubMed

Bioconjugate Chemistry

Article

pubs.acs.org/bc

In Vivo Detection of Phospholipase C by Enzyme-Activated Near-Infrared Probes

Theresa M. Mawn, Anatoliy V. Popov, Nancy J. Beardsley, Klara Stefflova,[†] Matthew Milkevitch,[‡] Gang Zheng,[§] and E. James Delikatny*

Department of Radiology, University of Pennsylvania, Philadelphia, Pennsylvania 19104, United States

ABSTRACT: In this article, the characterization of the first near-infrared (NIR) phospholipase-activated molecular beacon is reported, and its utility for *in vivo* cancer imaging is demonstrated. The probe consists of three elements: a phospholipid (PL) backbone to which the NIR fluorophore, pyropheophorbide *a* (Pyro), and the NIR Black Hole Quencher 3 (BHQ) were conjugated. Because of the close proximity of BHQ to Pyro, the Pyro-PtdEtn-BHQ probe is self-quenched until enzyme hydrolysis releases the fluorophore. The Pyro-PtdEtn-BHQ probe is highly specific to one isoform of phospholipase C, phosphatidylcholine-specific phospholipase C (PC-PLC), responsible for catabolizing phosphatidylcholine directly to phosphocholine. Incubation of Pyro-PtdEtn-BHQ *in vitro* with PC-PLC demonstrated a 150-fold increase in fluorescence that could be inhibited by the specific PC-PLC inhibitor tricyclodecan-9-yl xanthogenate (D609) with an IC_{50} of 34 ± 8 μM. Since elevations in phosphocholine have been consistently observed by magnetic resonance spectroscopy in a wide array of cancer cells and solid tumors, we assessed the utility of Pyro-PtdEtn-BHQ as a probe for targeted tumor imaging. Injection of Pyro-PtdEtn-BHQ into mice bearing DU145 human prostate tumor xenografts followed by *in vivo* NIR imaging resulted in a 4-fold increase in tumor radiance over background and a 2 fold increase in the tumor/muscle ratio. Tumor fluorescence enhancement was inhibited with the administration of D609. The ability to image PC-PLC activity *in vivo* provides a unique and sensitive method of monitoring one of the critical phospholipase signaling pathways activated in cancer, as well as the phospholipase activities that are altered in response to cancer treatment.

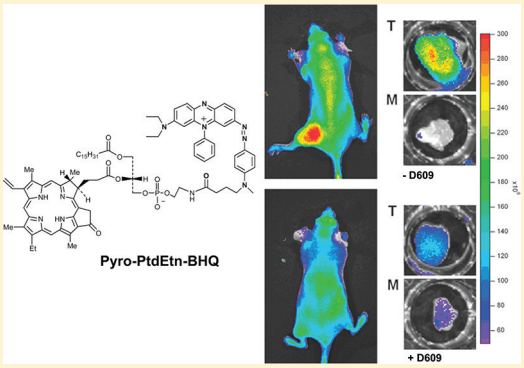

■ INTRODUCTION

Molecular imaging techniques offer the potential ability to detect cancer at a curable stage, to monitor and adjust patient treatments, and to improve the efficiency of cancer drug development.[1] Direct monitoring of a molecular target allows detailed elucidation of key metabolic pathways and specific cellular processes that become deregulated in cancer.[2−6] Lipids play an important role in the regulation of cellular responses and communication,[7] so it is not surprising that the lipid metabolic profile has been found to be altered in a variety of cancers. The development of probes for imaging lipid metabolism has been relatively unexplored but holds great promise for resolving and monitoring specific molecular targets for anticancer therapy.

Magnetic resonance spectroscopy (MRS) has been used extensively to study the biochemistry and physiology of cancer cells and solid tumors by observing changes in the lipid metabolites of phosphatidylcholine (PtdCho). Over the past two decades, ^{1}H- and ^{31}P-MRS have consistently revealed the presence of increased levels of phosphocholine (PC) in breast,[8−14] prostate,[13,15−18] and brain[8,13,16,19−21] cancer cells and solid tumors. Elevated levels of PC, in particular, have been correlated with the degree of malignancy,[22−24] and it has been shown that PC levels decrease in response to chemotherapeutic treatment.[25] Although elevations in PC have been attributed to up-regulation of choline transport and choline kinase activity,[22,25] there is also evidence that increased PtdCho catabolism may also play a role.[14,26,27] Phosphatidylcholine-specific phospholipase C (PC-PLC) hydrolyzes PtdCho to PC and diacylglycerol and has been implicated in contributing to the irregular choline metabolism in cancer.[26,28,29] It is of growing importance to resolve the source of PC as a potential marker for the malignant phenotype[10,30] and for assessing tumor response to therapy.[31,32]

In a previous paper, we reported the synthesis of a series of self-quenched near-infrared (NIR) fluorescent probes sensitive to the actions of phospholipases.[33] This follows from our studies in which the enzymatic activation of a protease-sensitive probe resulted in the separation of a fluorophore from a dark quencher leading to increased fluorescence.[34,35] In this article, we focus on one probe, Pyro-PtdEtn-BHQ (1-palmitoyl-2-pyropheophorbide-*sn*-glycero-3-phosphoethanolamine-BHQ-3), which is highly specific to PC-PLC, in order to directly examine the contribution of the catabolic pathway to increased levels of PC. The NIR fluorophore, pyropheophorbide *a* (Pyro; λ_{ex} = 410, 665 nm; λ_{em} = 670, 725 nm), is attached to the *sn*-2

Received: May 7, 2011
Revised: September 29, 2011
Published: October 31, 2011

position, and the NIR Black Hole Quencher 3 (BHQ, absorbance range: 620−730 nm) is conjugated to the headgroup. The close proximity of the quencher to the fluorophore results in fluorescence quenching. Upon enzymatic cleavage by PC-PLC, the fluorescent moiety is separated from the phospholipid, and fluorescence is restored. Results from a positive control, a fluorescent unquenched lipid analogue, Pyro-PtdEtn (1-palmitoyl-2-pyropheophorbide-*sn*-glycero-3-phosphoethanolamine), are also reported.

It is demonstrated that Pyro-PtdEtn-BHQ exhibits a marked specificity for PC-PLC and that it can be activated in cultured DU145 human prostate tumor cells and tumor xenografts. Moreover, fluorescence can be attenuated using tricyclodecan-9-yl xanthogenate (D609), a specific inhibitor to PC-PLC, both in solution and *in vivo*. These data indicate that the catabolic pathway of PC formation via PC-PLC may be an important contributor to the alterations in choline metabolism seen in cancer progression and development.

MATERIALS AND METHODS

Synthesis of Pyro-PtdEtn-BHQ and Pyro-PtdEtn. The detailed synthesis and characterization of a series of phospholipase-sensitive fluorophores has been published elsewhere.[33] Pyropheophorbide *a* (λ_{abs} = 665 nm, λ_{em} = 725 nm) was prepared from *Spirulina Pacifica* algae (Cyanotech Corporation, Kailua-Kona, HI, USA) according to a previously published procedure.[36] *N-tert*-butoxycarbonyl-1-palmitoyl-*sn*-glycero-3-phosphoethanolamine (Lyso-PtdEtn-N-Boc, Avanti Polar Lipids, Inc., Alabaster, AL) was acylated with Pyro in the presence of *N*-(3-dimethylaminopropyl)-N′-ethyl carbodiimide hydrochloride (EDC), and 4-dimethylaminopyridine (DMAP). N-Boc deprotection with trifluoroacetic acid resulted in the permanently fluorescent phospholipid analogue, Pyro-PtdEtn, at 30% yield (50 mg). Further N-acylation of Pyro-PtdEtn with BHQ succinimidyl ester hexafluorophosphate (BHQ-3-$SU^+PF_6^-$, λ_{abs} = 620−730 nm, Biosearch Technologies, Novato, CA) in the presence of triethylamine (Et_3N) in CH_2Cl_2 gave rise to Pyro-PtdEtn-BHQ at 15% yield (20 mg).

Phospholipases. Phospholipases were obtained from Sigma (St. Louis, MO), dissolved in Tris buffer (50 mM Tris-HCl, pH 7.4) and stored in aliquots at −20 °C. Mammalian phospholipase isoforms were used whenever available: $sPLA_2$ (type IB, porcine pancreas and bovine pancreas), otherwise bacterial isoforms were employed: PC-PLC (*Bacillus cereus*), PI-PLC (*B. cereus*), SMase (*B. cereus*), and PC-PLD (*Streptomyces chromofuscus*).

Lipid Dispersions. Pyro-PtdEtn-BHQ or Pyro-PtdEtn (ε = 110,000 M^{-1} cm^{-1} at 410 nm) was combined with PtdCho (chicken egg, Avanti Polar Lipids, Inc., Alabaster, AL) in chloroform and dried under a stream of nitrogen. Lipid films were rehydrated with buffer (50 mM Tris-HCL, pH 7.4), and small unilamellar vesicles were formed by sonication until an optically clear dispersion was obtained. For TLC and MALDI-TOF experiments, a concentration of 200 μM Pyro-PtdEtn-BHQ was used at a mole fraction of 0.05 in egg PtdCho. For kinetic experiments, a concentration of 1 μM Pyro-PtdEtn-BHQ was used at mole fractions of 0.002−0.04 in egg PtdCho.

TLC Assay. Aliquots (200 μL) of the sonicated Pyro-PtdEtn-BHQ/egg-PtdCho (MF 0.05) lipid dispersion were incubated at 37 °C with 1 U of enzyme: PC-PLC, PI-PLC, SMase, PC-PLD, type IA $sPLA_2$, or type IB $sPLA_2$. After 24 h, a sample from each aliquot was separated on an UV Silica Gel TLC plate using the solvent chloroform/methanol (100:15). Fluorescent bands due to cleavage were detected using a 385 nm UV lamp. The *Rf* of each band was compared to a control Pyro-PtdEtn-BHQ/lipid dispersion that had not been exposed to enzyme.

HPLC and MALDI-TOF Mass Spectrometry. Products of the Pyro-PtdEtn-BHQ-phospholipase cleavage experiments were separated using reverse-phase HPLC. The HPLC system consisted of a Waters 600 controller with a quaternary pump equipped with a Waters 2996 diode array detector (Waters Corp, Milford, CT) and a Zorbax 300SB-C3 column (4.6 × 150 mm, Agilent Corp, Santa Clara, CA). The flow rate of the mobile phase was 1.5 mL/min. The mobile phase composition was (A) acetonitrile, (B) 0.1 M triethylamine + acetic acid, pH 7, and (C) methanol. Solvent composition began with 80% solvent A and 20% solvent B, which was increased to 90% A and 10% B over 10 min. Conditions were then changed to 90% A and 10% C for 10 min followed by 90% C and 10% A over 60 min. The identity of isolated fragments was subsequently confirmed with MALDI-TOF MS using an Applied Biosystems Voyager DE Mass Spectrometer with positive mode ionization. The matrix consisted of α-cyano-4-hydroxycinnamic acid or 2-(4-hydroxyphenylazo)benzoic acid.

Confocal Microscopy Studies. Cells (1 × 10^5 cells/mL) were grown on Nunc chambered culture slides for 24 h and incubated for 1 h at 37 °C with 10 μL of 5 μM Pyro PL or Pyro-PtdEtn-BHQ in saline or saline as a control. The cells were rinsed, mounted, and observed via confocal microscopy on a Zeiss LSM 510 META confocal microscope with λ_{ex} = 633 nm and λ_{em} = 665−718 nm. The intensity density was quantified from each image using ImageJ software and normalized to the area occupied by cells.

Kinetics Analysis by Fluorescence Spectroscopy. A Molecular Devices SpectraMax M5 microplate reader was used to measure the fluorescence from 100 μL samples containing 1 μM substrate dispersed in egg-PtdCho vesicles in buffer (50 mM Tris-HCl, pH 7.4). Following enzyme addition, the initial rate measured in relative fluorescence units per minute (RFU/min) was determined using SoftMax Pro Software (Molecular Devices, Sunnyvale, CA) with λ_{ex} = 410 nm and λ_{em} = 675 nm.

Cell Culture. The human prostate carcinoma cell line, DU145, was maintained in MEM Eagle culture medium supplemented with 10% (v/v) fetal calf serum, 2 mM L-glutamine, and 1% penicillin/streptomycin and buffered with 20 mM sodium bicarbonate. Cultures were grown in 150 cm^2 filter cap tissue culture flasks using standard culture conditions of 37 °C and 5% CO_2 in air.

***In Vivo* NIR Fluorescence Imaging.** DU145 cells (5 × 10^6) were injected subcutaneously above the left hind legs of 4−6 week old athymic nude mice (NCI, Fort Dietrich, MD). Tumors were grown for 4−6 weeks until they reached a volume of 200−400 mm^3. Mice were fed low-fluorescent pellets (Labdiet 5 V02, Animal Specialties and Provisions, LLC, PA) for 1−3 days prior to imaging. Mice were anesthetized with 100 μL of ketamine (50 mg/mL) /acepromazine (5 mg/mL). Prescan visible and fluorescent images were taken with a Xenogen IVIS system using Cy5.5 fluorescence filters (λ_{ex} = 615−667 nm, λ_{em} = 695−770 nm), and an exposure time of 1 s. Following the prescan image, the mice were injected i.v. with 80 nmol Pyro-PtdEtn or Pyro-PtdEtn-BHQ solubilized in 50 mM Tris-HCl, pH 7.4, and 0.1% Tween-80 (200 μL/mouse). In inhibition experiments, D609 (Sigma-Aldrich, St. Louis, MO) was administered intraperitoneally at a dose of 50 μg/g body weight 30 min prior to and 30, 60, and 120 min post-injection

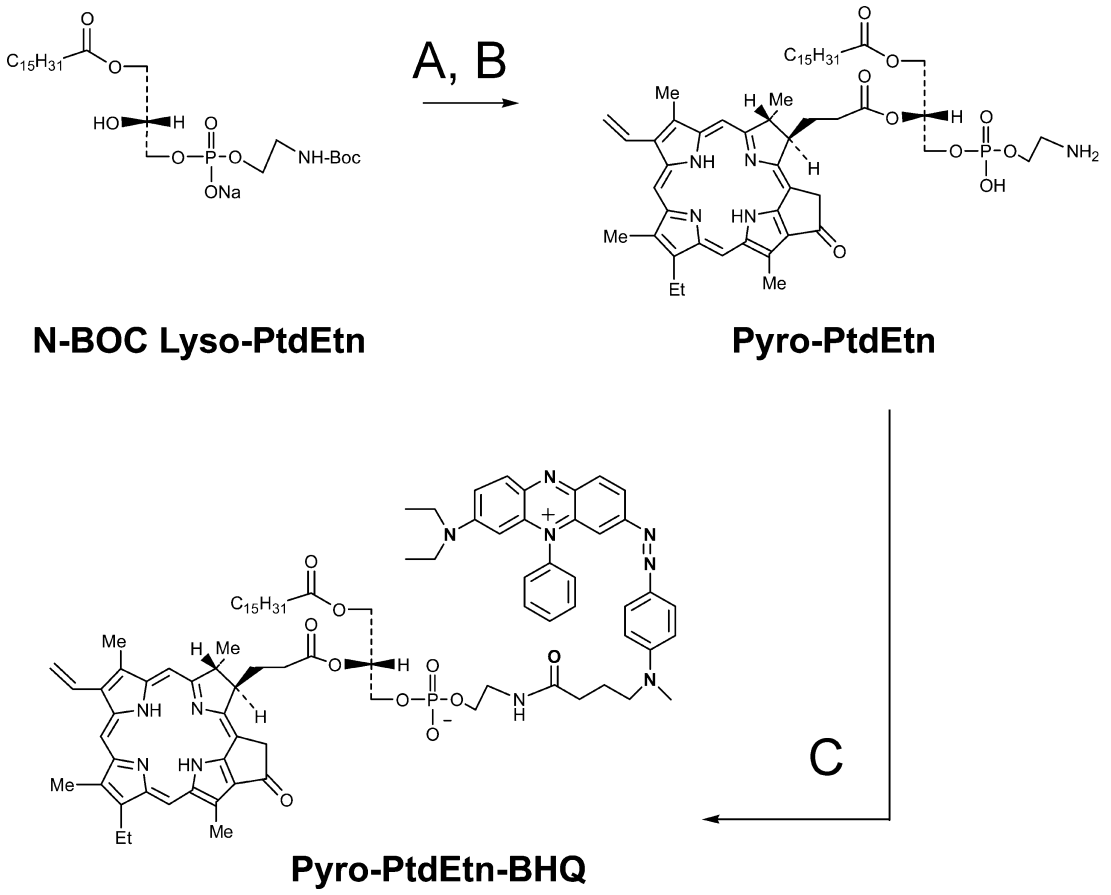

Figure 1. Synthesis of Pyro-PtdEtn and Pyro-PtdEtn-BHQ. (A) Pyro, EDC, DMAP, and CH_2Cl_2, at 25 °C, 72 h, argon (Ar); (B) TFA and CH_2Cl_2, at 0 °C, 4 h, Ar; (C) BHQ-3-SU$^+PF_6^-$, Et_3N, and CH_2Cl_2, at 25 °C, 12 h, Ar.

of Pyro-PtdEtn-BHQ.[37,38] Images were acquired every few minutes for the first 1.5 h, followed by every hour up to 6 h, and then again between 24 and 30 h. Background fluorescence was subtracted from all images. A region of interest was drawn around both the tumor and the contralateral muscle, and the average radiance was measured (photons/s/cm^2/sr). The tumor/muscle average radiance ratios were calculated at each time point.

Amplex Red Assay of PC-PLC Activity in Extracts of Tumor Xenografts. DU145 tumors were excised from euthanized mice and weighed (~90 mg). Tumors were sliced, minced, and transferred to 15 mL centrifuge tubes in 7 mL of cold PBS (without Ca^{2+} or Mg^{2+}). Samples were centrifuged at 7000 rpm for 8 min. PBS was removed, and pellets were lysed at 4 °C for 30 min with 0.5 mL of lysis buffer (50 mM Tris-HCl at pH 7.4, 1% Triton X-100, 1 Complete Mini protease inhibitor tablet, 1 mM EGTA, 2 mM EDTA, and 150 mM NaCl). The lysed suspensions were homogenized for 5 min and centrifuged at 13,500 rpm for 10 min, and the supernatant fraction was collected and stored at −80 °C. PC-PLC activity was determined by adding the thawed supernatant fraction to a reaction mixture containing 0.4 mM Amplex Red, 1 unit/mL horseradish peroxidase, 4 unit/mL alkaline phosphatase, 0.1 unit/mL choline oxidase, and 0.5 mM PtdCho in 1× Reaction Buffer (50 mM Tris-HCl, pH 7.4, 0.14 M NaCl, 10 mM dimethylglutarate, and 2 mM $CaCl_2$).[39] PC released from PtdCho by PC-PLC is converted to choline by alkaline phosphatase, which is further oxidized to form H_2O_2. In the presence of horseradish peroxidase, the H_2O_2 reacts with Amplex Red to generate the fluorophore, resorufin, which was detected using λ_{ex} = 560 nm and λ_{em} = 590 nm on the SpectraMax M5 plate reader.

Statistical Analysis. All data are presented as the mean ± SD. Statistical analysis of *in vivo* tumor/muscle average radiance was conducted using a Student's *t*-test. The test performed was two-tailed when testing Pyro-PtdEtn against Pyro-PtdEtn-BHQ (±D609) and one-tailed when testing Pyro-PtdEtn-BHQ against Pyro-PtdEtn-BHQ + D609. A p value ≤0.05 was considered to be significant.

RESULTS

Synthesis and Spectral Characteristics of Pyro-PtdEtn and Pyro-PtdEtn-BHQ. The synthesis of Pyro-PtdEtn and Pyro-PtdEtn-BHQ is presented in Figure 1. The close proximity of BHQ to Pyro, as well as the strong BHQ absorbance over the Pyro emission wavelength region, results in efficient contact and FRET quenching of this construct.

Specificity and Sensitivity. To determine probe specificity, Pyro-PtdEtn-BHQ was incubated for 24 h with a range of phospholipases: PC-PLC, phosphatidylinositol-specific PLC (PI-PLC), sphingomyelinase (SMase), phosphatidylcholine-specific phospholipase D (PC-PLD), type IA secretory phospholipase A_2 (sPLA$_2$), type IB sPLA$_2$ (porcine), and type IB sPLA$_2$ (bovine). TLC analysis showed that Pyro-PtdEtn-BHQ could be cleaved by PC-PLC, and to a lesser extent, SMase and PC-PLD (Figure 2) with the fluorescent Pyro moiety appearing under UV light as a red spot with a retention factor (*Rf*) of 0.9 (Columns 2 and 4). The sample

dx.doi.org/10.1021/bc200242v | *Bioconjugate Chem.* 2011, 22, 2434–2443

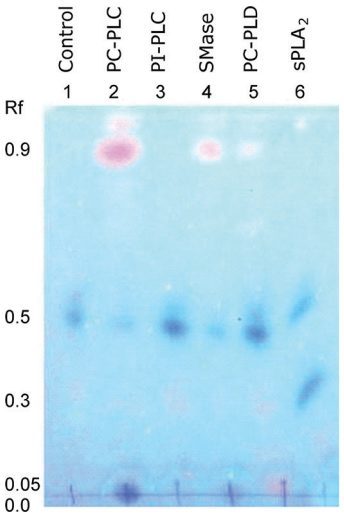

Figure 2. Specificity determined by TLC. Pyro-PtdEtn-BHQ/egg-PtdCho lipid dispersions were incubated with enzymes for 24 h and the products separated on a TLC plate using chloroform/methanol (100:15): 1, Control (no enzyme); 2, PC-PLC; 3, PI-PLC; 4, SMase; 5, PC-PLD; and 6, sPLA2 (IB, porcine). BHQ moieties were visible as blue spots, while fluorescent Pyro moieties were observed as red spots under UV excitation (385 nm). No enzyme activity was observed by PI-PLC, whereas sPLA2 (porcine type IB) cleavage showed 2 nonfluorescent spots. The observed cleaved products confirmed by HPLC followed by MALDI-TOF are as follows: *Rf* = 0.9, 1- acyl-2-pyropheophorbide glycerol (lanes 2, 4, and 5); *Rf* = 0.5, Pyro-PtdEtn-BHQ; *Rf* = 0.3, Lyso-Pyro- PtdEtn-BHQ (lane 6); *Rf* = 0.05 (red), 1-acyl-2-pyropheophorbide-3-phosphate (lane 5); *Rf* = 0.0 (blue), phospho-BHQ-3 (lanes 2, 4, and 5).

exposed to PC-PLD (Column 5) resulted in two fluorescent products, at *Rf* 0.9 and 0.05, while the uncleaved Pyro-PtdEtn-BHQ and the cleaved nonfluorescent product, phospho-BHQ-3, were visible as dark spots at *Rf* 0.5 and 0.0, respectively. No activity was observed with PI-PLC (Column 3). Type IB (porcine) $sPLA_2$ released one nonfluorescent product at *Rf* 0.3 (Column 6), whereas no cleavage was seen using either type IA $sPLA_2$ or type IB $sPLA_2$ (bovine).

To confirm these assignments, the TLC samples were analyzed by HPLC with UV−visible detection and MALDI-TOF MS (Figure 3). Figure 3A shows the HPLC chromatogram of Pyro-PtdEtn-BHQ, showing two closely separated peaks at retention times (RT) of 56.4 and 57.9 min. MALDI-TOF MS confirmed that the high RT peak corresponded to free Pyro-PtdEtn-BHQ (Table 1, calculated molecular weight (MW), 1497.8 Da; found, 1497.7 *m*/*z*), whereas the low RT peak (Figure 3D; found, 1498.2 *m*/*z*) also displayed a series of low MW ions from 500−800 *m*/*z* and may correspond to lipids from vesicle-encapsulated Pyro-PtdEtn-BHQ. Upon treatment with PC-PLC, we observed two cleavage products (Figure 3B). The corresponding UV−visible spectra (Figure 3C) showed that the first product (RT = 21.0 min) exhibited the absorbance spectrum of Pyro, whereas the second (RT = 53.4 min) exhibited the spectrum of BHQ. MALDI-TOF MS further validated that Pyro-PtdEtn-BHQ was cleaved by PC-PLC into two products that had MWs consistent with 1-palmitoyl-2-pyropheophorbide glycerol (calculated, 846.5 Da; found, 846.2 *m*/*z*) and phosphoethanolamine-BHQ-3 (calculated, 669.3 Da; found, 669.7 *m*/*z*), as shown in Figure 3E and F, respectively, and in Table 1. Incubation with SMase resulted in the same cleavage products (Table 1). MALDI-TOF MS also confirmed the existence of the two fluorescent products detected by HPLC in the sample treated with PC-PLD, the expected 1-palmitoyl-2-pyropheophorbide-*sn*-glycero-3-phosphate and 1-palmitoyl-2-pyropheophorbide glycerol, the same product released

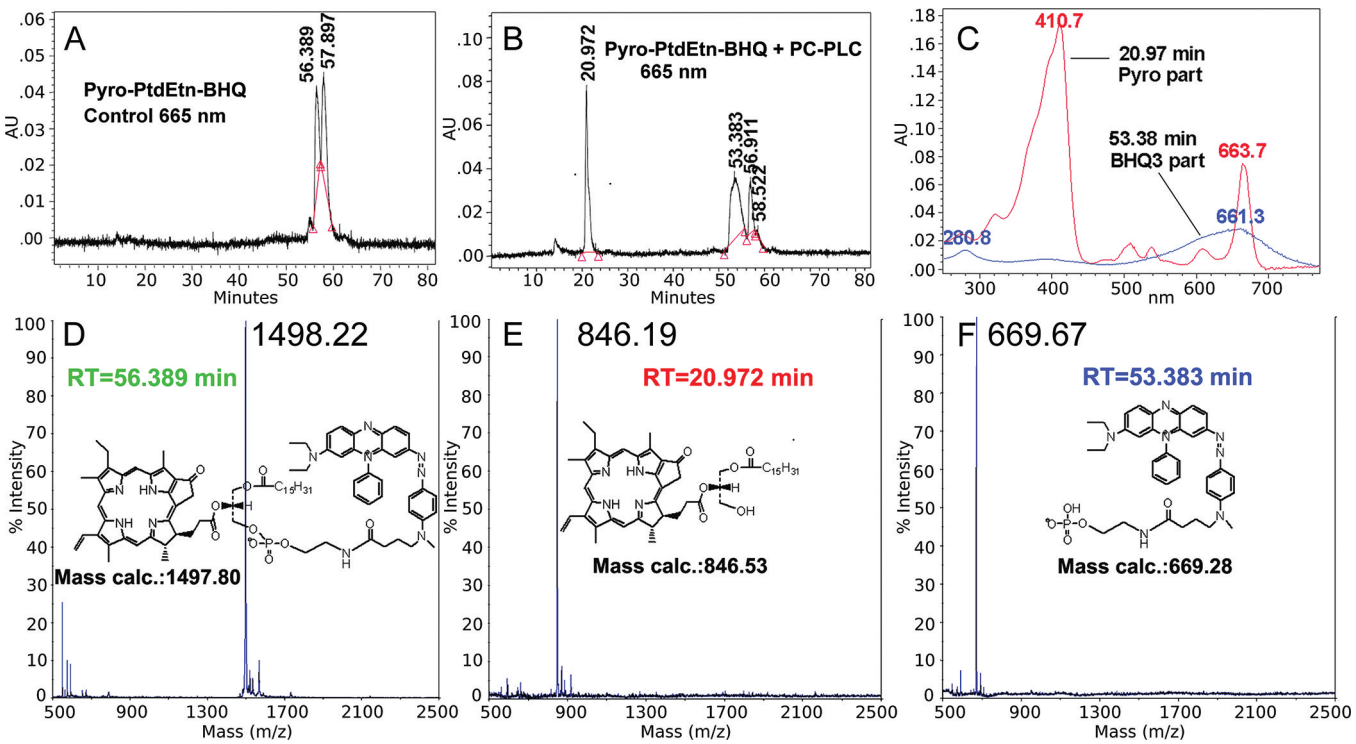

Figure 3. Validation of PC-PLC activation of Pyro-PtdEtn-BHQ. HPLC chromatogram of (A) Pyro-PtdEtn-BHQ and (B) cleavage products of Pyro-PtdEtn-BHQ from the actions of PC-PLC; (C) corresponding UV spectra of cleaved products; MALDI-TOF mass spectra and chemical structures of (D) Pyro-PtdEtn-BHQ and PC-PLC derived products: (E) 1-palmitoyl-2-pyropheophorbide glycerol and (F) phospho-BHQ-3.

dx.doi.org/10.1021/bc200242v | *Bioconjugate Chem.* 2011, 22, 2434−2443

Table 1. MALDI-TOF Parent Ion Peaks and Calculated Masses for Pyro-PtdEtn-BHQ and Enzymatic Cleavage Products

enzyme	product(s)	calculated exact mass (Da)	observed mass (m/z)
none	1-palmitoyl-2-pyropheophorbide-*sn*-glycero-3-phosphoethanolamine-BHQ-3 (pyro-PtdEtn-BHQ)	1497.8	1497.7
			1498.2
PC-PLC	1-palmitoyl-2-pyropheophorbide glycerol	846.5	846.2
	phosphoethanolamine-BHQ-3	669.3	669.7
SMase	1-palmitoyl-2-pyropheophorbide glycerol	846.5	846.2
	phosphoethanolamine-BHQ-3	669.3	669.7
PC-PLD	1-palmitoyl-2-pyropheophorbide 3-phosphate	926.5	926.4
	BHQ-3 ethanolamide	590.3	591.4
			590.4
	1-palmitoyl-2-pyropheophorbide glycerol	846.5	846.2
	phosphoethanolamine-BHQ-3	669.3	669.7
sPLA2 1B	2-pyropheophorbide-*sn*-glycero-3-BHQ-3	1259.6	1258.5
	palmitic acid	256.2	256.3
			257.3

by PC-PLC (Table 1), suggesting a cross-reactivity or a PC-PLC impurity. We found the nonfluorescent product released by $sPLA_2$ (type IB, porcine) to be the result of phospholipase A_1 activity having a molecular weight consistent with 2-pyropheophorbide-*sn*-glycero-3-BHQ-3 (Table 1), presumably also due to the lack of enzyme specificity or enzyme impurity.

Although PC-PLC, SMase, and PLD all demonstrated the ability to hydrolyze Pyro-PtdEtn-BHQ after incubation for 24 h, observation of these reactions by fluorescence spectroscopy revealed that the kinetics of these reactions were very different (Figure 4A).

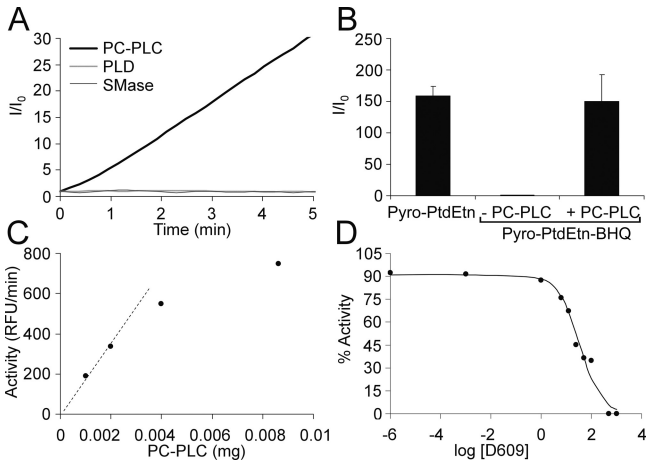

Figure 4. Characterization of Pyro-PtdEtn-BHQ kinetics. (A) Time-dependent increase in fluorescence of 1 μM Pyro-PtdEtn-BHQ incubated with 10 U each of PC-PLC, PLD, or SMase; (B) fold increase in fluorescence of 1 μM Pyro-PtdEtn-BHQ before and after complete activation by PC-PLC, as compared to that of Pyro-PtdEtn at equal concentrations (error bars represent s.d., n = 3); (C) dependence of fluorescence release from Pyro-PtdEtn-BHQ on PC-PLC concentration; (D) inhibition of PC-PLC activity toward 1 μM Pyro-PtdEtn-BHQ by D609 (IC_{50} = 34 ± 8 μM).

The addition of PC-PLC (10 U) to 1 μM Pyro-PtdEtn-BHQ dispersed in egg-PtdCho vesicles (MF 0.02) led to a 30-fold increase in fluorescence within 5 min. In contrast, the fluorescence released by PC-PLD and SMase was negligible even after 1 h, indicating a remarkable sensitivity of Pyro-PtdEtn-BHQ for PC-PLC. As shown in Figure 4B, the complete hydrolysis of Pyro-PtdEtn-BHQ by PC-PLC *in vitro* resulted in a ~150-fold fluorescence increase, equaling the fluorescence of Pyro-PtdEtn at equal concentrations.

We determined the dependence of activity on enzyme concentration by adding increasing amounts of PC-PLC to 1 μM Pyro-PtdEtn-BHQ in egg-PtdCho dispersions (MF 0.003). The activity of PC-PLC with Pyro-PtdEtn-BHQ (Figure 4C) increased with enzyme and was linear up to 0.002 mg (0.5 U) of enzyme.

The rate of Pyro-PtdEtn-BHQ hydrolysis could be inhibited by D609, a specific PC-PLC inhibitor.[40] Activity was measured as a function of D609 concentration after the addition of 0.5 U PC-PLC (Figure 4D). Complete inhibition was achieved with 500 μM D609 and an IC_{50} of 34 ± 8 μM was determined.

Probe Uptake in Cancer Cells. To confirm the cellular uptake of Pyro-PtdEtn-BHQ, confocal fluorescence microscopy studies were performed on DU145 human prostate cancer cells incubated with Pyro-PtdEtn, Pyro-PtdEtn-BHQ, or PBS as a control (Figure 5). Pyro-PtdEtn-treated DU145 cells exhibited

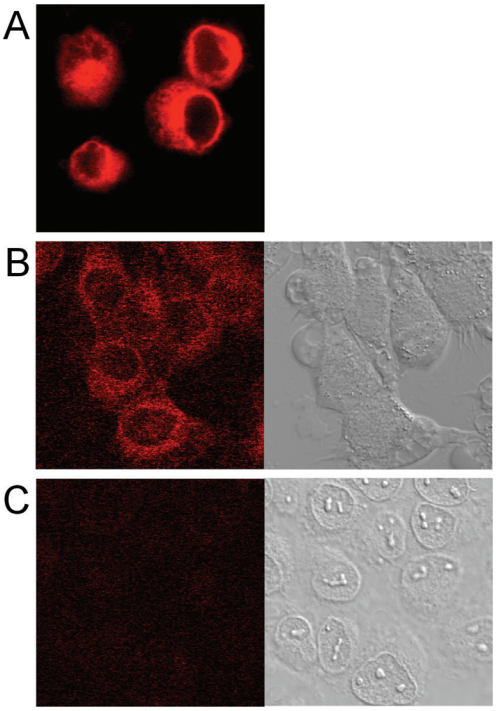

Figure 5. Confocal microscopy studies. Fluorescence (Left) and bright field (Right) micrographs of DU145 cells incubated for 1 h with (A) 5 μM Pyro-PtdEtn, (B) 5 μM Pyro-PtdEtn-BHQ, or (C) PBS as a control.

dx.doi.org/10.1021/bc200242v | *Bioconjugate Chem.* 2011, 22, 2434–2443

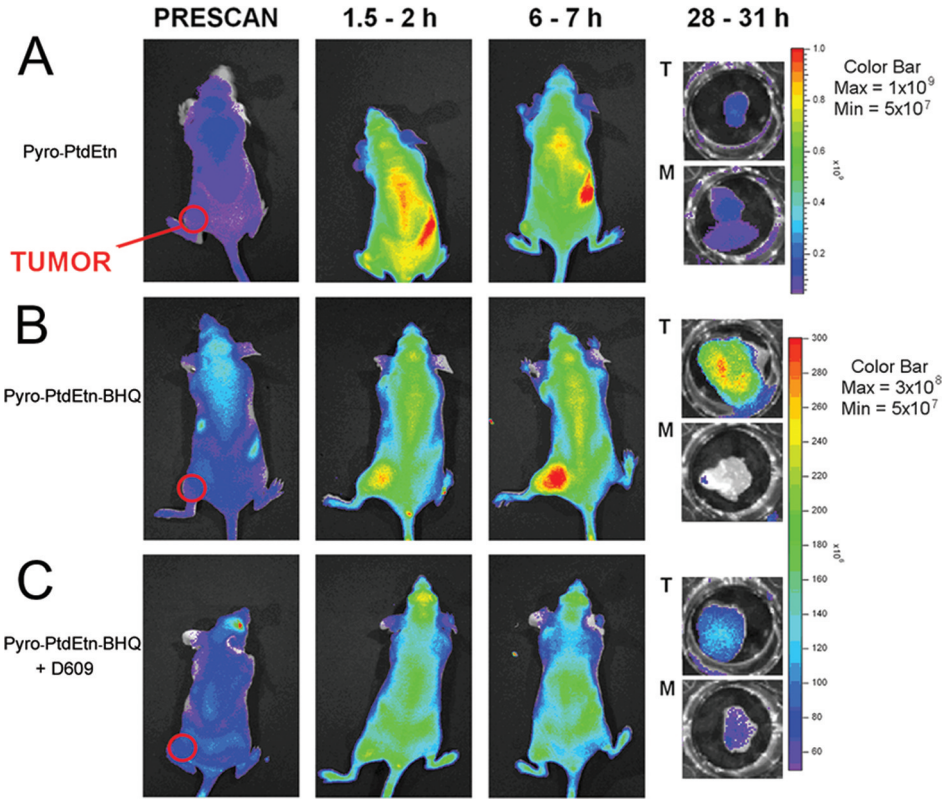

Figure 6. *In vivo* imaging of Pyro-PtdEtn, Pyro-PtdEtn-BHQ, and Pyro-PtdEtn-BHQ + D609 treatment. Nude mice bearing DU145 tumors on the left hind flank received 80 nmol i.v. of (A) Pyro-PtdEtn or (B and C) Pyro-PtdEtn-BHQ dispersed in 0.1 μM Tween-80. Mice in (C) received additional D609 injections (50 μg/g body weight, i.p.) at −30, 30, 60, and 120 min postinjection of Pyro-PtdEtn-BHQ. Images are shown at prescan, 1.5−2 h, and 6−7 h. The tumor (T) and muscle (M) tissues from each mouse were excised at 28−31 h.

a strong predominantly cytoplasmic fluorescent signal (Figure 5A). DU145 cells incubated with Pyro-PtdEtn-BHQ exhibited perinuclear and punctate cytoplasmic fluorescence that was approximately 8-fold less intense, due to differential cell uptake, incomplete intracellular activation, or quenching by BHQ (Figure 5B). Fluorescence in cells incubated with Pyro-PtdEtn-BHQ was approximately 10-fold more intense than DU145 cells incubated only with PBS (Figure 5C).

***In Vivo* Imaging of PC-PLC Activity.** We evaluated the efficacy of Pyro-PtdEtn-BHQ as a potential fluorescent imaging agent for detecting PC-PLC activity *in vivo*. Nude mice bearing DU145 human prostate tumor xenografts were injected with either Pyro-PtdEtn-BHQ or Pyro-PtdEtn as a positive control. Fluorescence images were acquired over the first 6 h and continued the next day between 24 and 30 h. Pyro-PtdEtn exhibited fast circulation throughout the body, accumulating primarily in the stomach, liver, and intestines (Figure 6A). By 6 h, the substrate was clearing through the digestive tract. By 28 h, very little radiance remained in the tumor or the contralateral muscle, as seen in the excised tissues in Figure 6 (T, tumor; M, muscle). Injection of Pyro-PtdEtn-BHQ, however, led to a gradual increase in tumor radiance within 1.5 h (Figure 6B) that was greatly increased at 6 h. At 30 h, we could still observe a high level of radiance in the excised tissue relative to the contralateral muscle tissue. Note that the Pyro-PtdEtn radiance detected *in vivo* is ∼3-fold higher than that of the cleaved Pyro-PtdEtn-BHQ radiance, which suggests that complete hydrolysis of Pyro-PtdEtn-BHQ is not being achieved.

In order to validate that the increase in tumor radiance after Pyro-PtdEtn-BHQ injection was due to PC-PLC activation, mice were injected with the PC-PLC inhibitor D609. As expected, D609 treatment inhibited *in vivo* activation of Pyro-PtdEtn-BHQ, resulting in reduced tumor radiance (Figure 6C). At 31 h, the excised tumor tissue exhibited half as much radiance as that found without D609 treatment.

Representative time dependence of the tumor and contralateral muscle radiance measurements for Pyro-PtdEtn, Pyro-PtdEtn-BHQ, and Pyro-PtdEtn-BHQ + D609 are shown in Figure 7. Administration of Pyro-PtdEtn led to a sharp increase in tumor and muscle radiance, reaching a maximum tumor radiance of ∼10-fold over baseline at 30 min, followed by an immediate drop as the probe begins to clear, and return to prescan level by 24 h post-injection (Figure 7A). In contrast, Pyro-PtdEtn-BHQ tumor radiance gradually increased ∼4-fold over baseline during the first 4 h and was maintained continually up to 24 h before beginning to clear from the tumor (Figure 7B). From 2−24 h, the tumor radiance increased to about 2.5-fold greater than that in the contralateral muscle and was significantly greater at 24 h ($p < 0.05$). Pre- and post-treatment with D609 caused an overall attenuation of tumor radiance as soon as 2 h after injection and continued to suppress probe activation until clearance at 28 h (Figure 7C). The average of the tumor/muscle radiance ratios for each condition are presented in Figure 7D. Here a 2-fold increase in tumor/muscle ratio was observed by 24 h in mice treated with Pyro-PtdEtn-BHQ. D609 treatment significantly inhibited the activation of Pyro-PtdEtn-BHQ at the 24 h time point ($p < 0.05$), decreasing the tumor/muscle ratio back to baseline.

At the end of the experiment (28−31 h post-injection), the organs were excised and imaged on the IVIS-100 in 24 well

dx.doi.org/10.1021/bc200242v | *Bioconjugate Chem.* 2011, 22, 2434−2443

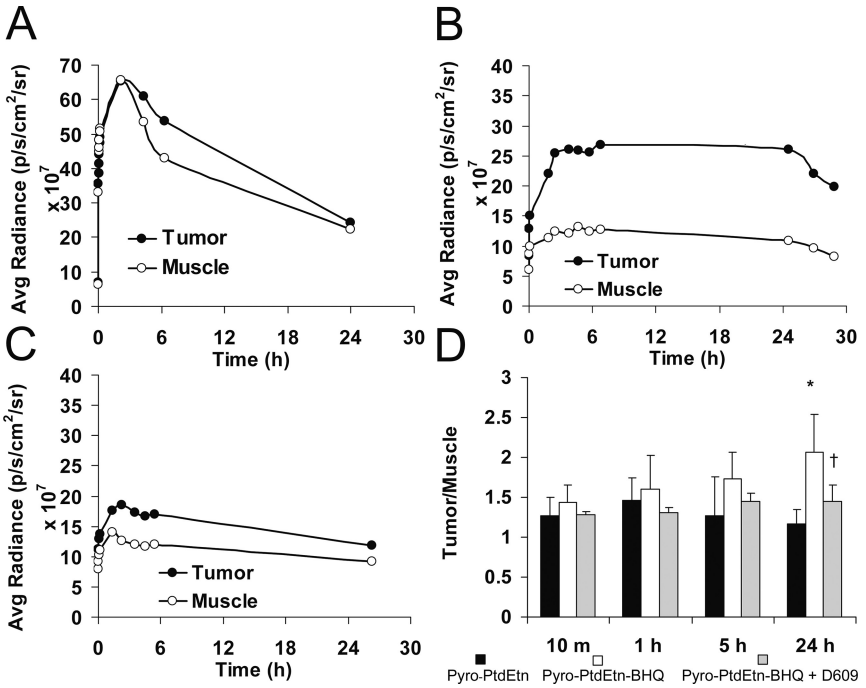

Figure 7. Representative time courses of measured tumor and muscle average radiances. The average radiance from the tumor and muscle tissue and was quantified in mice injected with (A) Pyro-PtdEtn, (B) Pyro-PtdEtn-BHQ, and (C) Pyro-PtdEtn-BHQ + D609. (D) Tumor/muscle average radiance. The average tumor radiance was normalized to muscle for Pyro-PtdEtn (n = 5), Pyro- PtdEtn-BHQ (n = 5), and Pyro-PtdEtn-BHQ + D609 treatment (n = 3). Error bars represent SD. * Significantly (p = 0.011) different from Pyro-PtdEtn. † Significantly (p = 0.024) different from Pyro- PtdEtn-BHQ without D609 treatment.

plates (Table 2). These data show major residual fluorescence in the stomach, intestine, and liver and indicate that these probes are excreted via the bile, liver, and stool as would be expected for a lipid soluble probe.

Validation of PC-PLC Activity in Extracts of DU145 Tumor Xenografts. To validate the presence of PC-PLC activity in DU145 tumor xenografts, the Amplex Red PC-PLC Assay Kit (Invitrogen, Eugene, OR) was used in excised tumor extracts. PC-PLC activity was shown to increase linearly as a function of total supernatant protein (Figure 8A) as detected by increases in resorufin fluorescence (Figure 8A). This activity was shown to decrease as a function of D609 concentration (Figure 8B).

DISCUSSION

In this article, we report a direct, sensitive, and feasible method for detecting PC-PLC activity employing a self-quenched phospholipid analogue that restores NIR fluorescence upon enzymatic hydrolysis. A high specificity was found for PC-PLC in solution studies, and enzyme activity was detected in cultured DU145 human prostate cells and *in vivo* using a DU145 tumor xenograft mouse model.

Although activatable fluorescent probes to detect phospholipase activity *in vitro* have been previously reported,[41−47] Pyro-PtdEtn-BHQ is unique in that it contains the NIR fluorochrome, pyropheophorbide *a*, which allows for increased photon penetration through biological tissue in a spectral region where tissue autofluorescence is markedly reduced.[48] This modification means that *in vivo* NIR optical detection of phospholipase activity has been made possible. Pyropheophorbide was chosen as the fluorophore for these studies because when conjugated, it is both neutral and hydrophobic, two properties necessary for the lipid-based probe to be incorporated into membranes. However, pyropheophorbide *a* is also a known photosensitizer, with a high singlet oxygen quantum yield, opening the possibility that this and other related probes could be used for photodynamic therapy to treat tumors *in vivo*.

This article shows that Pyro-PtdEtn-BHQ is highly specific to PC-PLC, when compared to several other phospholipase isoforms. As a phospholipid analogue, Pyro-PtdEtn-BHQ was also shown to be a substrate for PC-PLD and SMase, although with much less activity. Thus, it is possible that increases in activity could arise from activation by other enzymes, at a much slower rate. The inhibition studies with D609 would indicate that that is probably not the case. However, it is known that enzyme specificity and affinity for phospholipase-sensitive probes can be adjusted by altering the hydrophobicity and the length of the intervening fatty acyl chain at the *sn*-2 position.[33,49−51] We are currently in the process of synthesizing and testing a range of phospholipase probes of varying enzyme specificities and NIR fluorochromes, which will allow for multispectral detection of several phospholipases simultaneously.[33] This proposed molecular imaging strategy will lead to the development of probes specific to other important phospholipases and allow us to test these hypotheses in detail.

In this study, some bacterial isoforms of phospholipases were used for *in vitro* testing. This is due to the commercial unavailability of mammalian isoforms of these enzymes. A controversy also exists in the literature as to the origin of PC-PLC activity in mammals, as a mammalian isoform of this protein has never been cloned. However, isoforms have been isolated from mammalian sources.[52,53] There is also substantial evidence that the mammalian PC-PLC has functional similarity to the bacterial isoform. PC-PLC activity, as measured by D609-sensitive PC release from PtdCho, has been demonstrated in

Table 2. Fluorescence Intensity Observed in Excised Organs[a]

probe	organ/ adrenal glands	kidney	liver	spleen	heart	intestine	lung	muscle	stomach	tumor	pancreas
Pyro-PtdEtn (5)	$2.40\pm0.29\times10^9$	$6.09\pm2.47\times10^9$	$1.45\pm0.61\times10^{10}$	$4.67\pm1.50\times10^9$	$2.67\pm0.76\times10^9$	$1.85\pm1.03\times10^{10}$	$4.12\pm1.61\times10^9$	$2.48\pm1.20\times10^9$	$1.19\pm0.30\times10^{10}$	$3.71\pm1.96\times10^9$	$3.70\pm1.71\times10^9$
Pyro-PtdEtn-BHQ (5)	$1.70\pm0.62\times10^9$	$3.25\pm0.66\times10^9$	$8.96\pm2.16\times10^9$	$2.68\pm0.78\times10^9$	$1.78\pm0.64\times10^9$	$1.18\pm1.06\times10^{10}$	$2.00\pm0.56\times10^9$	$1.72\pm0.67\times10^9$	$1.56\pm0.46\times10^{10}$	$3.44\pm1.40\times10^9$	$2.54\pm0.91\times10^9$
Pyro-PtdEtn-BHQ + D609 (2)	$9.80\pm0.25\times10^8$	$2.55\pm0.54\times10^9$	$1.02\pm0.19\times10^{10}$	$1.90\pm0.46\times10^9$	$1.22\pm0.21\times10^9$	$2.09\pm0.74\times10^{10}$	$1.41\pm0.55\times10^9$	$1.27\pm0.34\times10^9$	$1.97\pm1.11\times10^{10}$	$1.68\pm0.02\times10^9$	$1.55\pm0.33\times10^9$

[a]Data are expressed as photon flux (photons/s). The numbers of animals for each condition are in parentheses. Organs were removed from mice 28−31 h after injection of the probe and imaged in 24-well plates using the IVIS-100 system. The data show that residual fluorescence remains predominantly in the liver, intestine, and stomach, indicating excretion via the liver and stool.

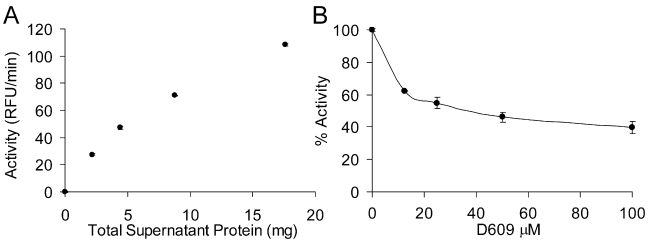

Figure 8. PC-PLC activity measured by Amplex Red. (A) Activity measured in relative fluorescence units per minute (RFU/min) as a function of protein (mg) from extracts of DU145 tumor xenografts. (B) Inhibition of PC-PLC activity in supernatants by D609.

cytoplasmic extracts of NIH-3T3 cells.[26] Polyclonal antibodies against *B. cereus* PC-PLC have been used to detect the translocation of a cross-reactive mammalian PC-PLC from the cytosol in control cells to the plasma membrane in oncogene-transformed cells.[26] An increased plasma membrane PC-PLC expression has also been shown to accompany tumor progression in ovarian cancer cell lines.[54] This PC-PLC activity could be measured with the Amplex Red assay and was sensitive to the action of D609. Our imaging results are consistent with these studies in that Pyro-PtdEtn-BHQ detected the presence of a D609-sensitive PC-PLC activity in DU145 tumors, which could be confirmed in extracts with the Amplex Red assay. We hope that the development of this probe will allow further investigation into the origins of PC-PLC activity and aid in the resolution of this controversy.

One of the added benefits of using enzyme-activated fluorescent imaging probes is the advantage of inherent signal amplification.[55,56] Our solution studies demonstrate an increase in fluorescence up to 150-fold greater than background. *In vivo*, although affected by the absorbance and scattering effects of biological tissue, an ∼4-fold increase in radiance was observed and a 2-fold increase in tumor to muscle fluorescence ratio. This signal increase over the background compares well with other recently reported enzyme-activated NIR probes used for imaging tumors *in vivo*, such as a cathepsin-sensitive probe[56] and a caspase 1 selective probe,[57] which display 3−4-fold and 1.7-fold tumor increases, respectively. These results establish Pyro-PtdEtn-BHQ as an excellent candidate for molecular imaging.

The *in vivo* results described in this work indicate that PC-PLC may be an important molecular marker for cancer. The additional coregistration of images obtained using phospholipase-activated NIR fluorescent probes with choline metabolite levels obtained from *in vivo* MRS could critically impact the field of cancer detection by offering a sensitive and specific method of examining the lipid catabolic pathways linked to the malignant phenotype.

AUTHOR INFORMATION

Corresponding Author

*Molecular Imaging Laboratory, Department of Radiology, University of Pennsylvania School of Medicine, Room 284, Chemistry Building 1958 Wing, 231 South 34th St., Philadelphia, PA 19104. Phone: (215) 898-3105. Fax: (215) 746-8764. E-mail: delikatn@mail.med.upenn.edu.

Present Addresses

[†]Cancer Research UK, Cambridge Research Institute, Cambridge, CB2 0RE, United Kingdom.

‡School of Science and Health, Philadelphia University, Philadelphia, PA 19144.
§Ontario Cancer Institute/University Health Network, MaRS Center, Toronto, ON, M5G 1L7, Canada.

■ ACKNOWLEDGMENTS

This work was supported by the National Cancer Institute (NCI) grants R01 CA114347 and R01 CA129176, National Institute of Biomedical Imaging and Bioengineering (NIBIB) grant R21 EB002537, the Small Animal Imaging Resource Program (SAIRP) grant R24 CA83105, the Metabolic Magnetic Resonance Research and Computing Center (MMRRCC) training grant T32-HL07614, and the NIH Research Resource grant P41 RR002305. Imaging was performed at the University of Pennsylvania Small Animal Imaging Facility (SAIF) Optical/Bioluminescence Core, supported by NIH grant CA105008, and we are grateful to Dr. Y. Yvette Liu for her technical assistance.

■ REFERENCES

(1) Weissleder, R. (2006) Molecular imaging in cancer. *Science 312*, 1168−11671.
(2) Stefflova, K., Chen, J., Li, H., and Zheng, G. (2006) Targeted photodynamic therapy agent with a built-in apoptosis sensor for in vivo near-infrared imaging of tumor apoptosis triggered by its photosensitization in situ. *Mol. Imaging 5*, 520−532.
(3) Blasberg, R. G. (2003) Molecular imaging and cancer. *Mol. Cancer Ther. 2*, 335−343.
(4) Mahmood, U., and Weissleder, R. (2003) Near-infrared optical imaging of proteases in cancer. *Mol. Cancer Ther. 2*, 489−496.
(5) Stefflova, K., Chen, J., and Zheng, G. (2007) Using molecular beacons for cancer imaging and treatment. *Front. Biosci. 12*, 4709−4721.
(6) Pham, W., Choi, Y., Weissleder, R., and Tung, C.-H. (2004) Developing a peptide-based near-infrared molecular probe for protease sensing. *Bioconjugate Chem. 15*, 1403−1407.
(7) Eyster, K. M. (2007) The membrane and lipids as integral participants in signal transduction: lipid signal transduction for the non-lipid biochemist. *Adv. Physiol. Educ. 31*, 5−16.
(8) Podo, F. (1999) Tumour phospholipid metabolism. *NMR Biomed. 12*, 413−439.
(9) Jacobs, M. A., Barker, P. B., Bottomley, P. A., Bhujwalla, Z., and Bluemke, D. A. (2004) Proton magnetic resonance spectroscopic imaging of human breast cancer: A preliminary study. *J. Magn. Reson. Imaging 19*, 68−75.
(10) Singer, S., Souza, K., and Thilly, W. G. (1995) Pyruvate utilization, phosphocholine and adenosine triphosphate (ATP) are markers of human breast tumor progression: a 31P- and 13C-nuclear magnetic resonance (NMR) spectroscopy study. *Cancer Res. 55*, 5140−5145.
(11) Katz-Brull, R., and Degani, H. (1996) Kinetics of choline transport and phosphorylation in human breast cancer cells; NMR application of the zero trans method. *Anticancer Res. 16*, 1375−1380.
(12) Gribbestad, I. S., Sitter, B., Lundgren, S., Krane, J., and Axelson, D. (1999) Metabolite composition in breast tumors examined by proton nuclear magnetic resonance spectroscopy. *Anticancer Res. 19*, 1737−1746.
(13) Negendank, W. (1992) Studies of human tumors by MRS: a review. *NMR Biomed. 5*, 303−324.
(14) Glunde, K., Jie, C., and Bhujwalla, Z. M. (2004) Molecular causes of the aberrant choline phospholipid metabolism in breast cancer. *Cancer Res. 64*, 4270−4276.
(15) Ackerstaff, E., Pflug, B. R., Nelson, J. B., and Bhujwalla, Z. M. (2001) Detection of increased choline compounds with proton nuclear magnetic resonance spectroscopy subsequent to malignant transformation of human prostatic epithelial cells. *Cancer Res. 61*, 3599−3603.
(16) Kurhanewicz, J., Vigneron, D. B., and Nelson, S. J. (2000) Three-dimensional magnetic resonance spectroscopic imaging of brain and prostate cancer. *Neoplasia 2*, 166−189.
(17) Swindle, P., McCredie, S., Russell, P., Himmelreich, U., Khadra, M., Lean, C., and Mountford, C. (2003) Pathologic characterization of human prostate tissue with proton MR spectroscopy. *Radiology 228*, 144−151.
(18) Milkevitch, M., Shim, H., Pilatus, U., Pickup, S., Wehrle, J. P., Samid, D., Poptani, H., Glickson, J. D., and Delikatny, E. J. (2005) Increases in NMR-visible lipid and glycerophosphocholine during phenylbutyrate-induced apoptosis in human prostate cancer cells. *Biochim. Biophys. Acta 1734*, 1−12.
(19) Bhakoo, K. K., Williams, S. R., Florian, C. L., Land, H., and Noble, M. D. (1996) Immortalization and transformation are associated with specific alterations in choline metabolism. *Cancer Res. 56*, 4630−4635.
(20) Li, X., Lu, Y., Pirzkall, A., McKnight, T., and Nelson, S. J. (2002) Analysis of the spatial characteristics of metabolic abnormalities in newly diagnosed glioma patients. *J. Magn. Reson. Imaging 16*, 229−237.
(21) Maris, J. M., Evans, A. E., McLaughlin, A. C., D'Angio, G. J., Bolinger, L., Manos, H., and Chance, B. (1985) 31P nuclear magnetic resonance spectroscopic investigation of human neuroblastoma in situ. *N. Engl. J. Med. 312*, 1500−1505.
(22) Eliyahu, G., Kreizman, T., and Degani, H. (2007) Phosphocholine as a biomarker of breast cancer: molecular and biochemical studies. *Int. J. Cancer 120*, 1721−1730.
(23) Katz-Brull, R., Seger, D., Rivenson-Segal, D., Rushkin, E., and Degani, H. (2002) Metabolic markers of breast cancer: enhanced choline metabolism and reduced choline-ether-phospholipid synthesis. *Cancer Res. 62*, 1966−1970.
(24) Aboagye, E. O., and Bhujwalla, Z. M. (1999) Malignant transformation alters membrane choline phospholipid metabolism of human mammary epithelial cells. *Cancer Res. 59*, 80−84.
(25) Al-Saffar, N. M., Troy, H., Ramirez de Molina, A., Jackson, L. E., Madhu, B., Griffiths, J. R., Leach, M. O., Workman, P., Lacal, J. C., Judson, I. R., and Chung, Y. L. (2006) Noninvasive magnetic resonance spectroscopic pharmacodynamic markers of the choline kinase inhibitor MN58b in human carcinoma models. *Cancer Res. 66*, 427−434.
(26) Podo, F., Ferretti, A., Knijn, A., Zhang, P., Ramoni, C., Barletta, B., Pini, C., Baccarini, S., and Pulciani, S. (1996) Detection of phosphatidylcholine-specific phospholipase C in NIH-3T3 fibroblasts and their H-ras transformants: NMR and immunochemical studies. *Anticancer Res. 16*, 1399−1412.
(27) Iorio, E., Ricci, A., Bagnoli, M., Pisanu, M. E., Castellano, G., Di Vito, M., Venturini, E., Glunde, K., Bhujwalla, Z. M., Mezzanzanica, D., Canevari, S., and Podo, F. (2010) Activation of phosphatidylcholine cycle enzymes in human epithelial ovarian cancer cells. *Cancer Res. 70*, 2126−2135.
(28) Ferretti, A., Podo, F., Carpinelli, G., Chen, L., Borghi, P., and Masella, R. (1993) Detection of neutral active phosphatidylcholine-specific phospholipase C in Friend leukemia cells before and after erythroid differentiation. *Anticancer Res. 13*, 2309−2317.
(29) Wu, X., Lu, H., Zhou, L., Huang, Y., and Chen, H. (1997) Changes of phosphatidylcholine-specific phospholipase C in hepatocarcinogenesis and in the proliferation and differentiation of rat liver cancer cells. *Cell Biol. Int. 21*, 375−381.
(30) Gelmon, K. A., Eisenhauer, E. A., Harris, A. L., Ratain, M. J., and Workman, P. (1999) Anticancer agents targeting signaling molecules and cancer cell environment: challenges for drug development? *J. Natl. Cancer Inst. 91*, 1281−1287.
(31) Beloueche-Babari, M., Chung, Y. L., Al-Saffar, N. M., Falck-Miniotis, M., and Leach, M. O. (2010) Metabolic assessment of the action of targeted cancer therapeutics using magnetic resonance spectroscopy. *Br. J. Cancer 102*, 1−7.
(32) Podo, F., Canevari, S., Canese, R., Pisanu, M. E., Ricci, A., and Iorio, E. (2011) MR evaluation of response to targeted treatment in cancer cells. *NMR Biomed. 24*, 648−672.

(33) Popov, A. V., Mawn, T. M., Kim, S., Zheng, G., and Delikatny, E. J. (2010) Design and synthesis of phospholipase C and A2-activatable near-infrared fluorescent smart probes. *Bioconjugate Chem. 21*, 1724−1727.
(34) Zheng, G., Chen, J., Stefflova, K., Jarvi, M., Li, H., and Wilson, B. C. (2007) Photodynamic molecular beacon as an activatable photosensitizer based on protease-controlled singlet oxygen quenching and activation. *Proc. Natl. Acad. Sci. U.S.A. 104*, 8989−8994.
(35) Stefflova, K., Chen, J., Marotta, D., Li, H., and Zheng, G. (2006) Photodynamic therapy agent with a built-in apoptosis sensor for evaluating its own therapeutic outcome in situ. *J. Med. Chem. 49*, 3850−3856.
(36) Zheng, G., Li, H., Zhang, M., Lund-Katz, S., Chance, B., and Glickson, J. D. (2002) Low-density lipoprotein reconstituted by pyropheophorbide cholesteryl oleate as target-specific photosensitizer. *Bioconjugate Chem. 13*, 392−396.
(37) Ansari, M. A., Joshi, G., Huang, Q., Opii, W. O., Abdul, H. M., Sultana, R., and Butterfield, D. A. (2006) In vivo administration of D609 leads to protection of subsequently isolated gerbil brain mitochondria subjected to in vitro oxidative stress induced by amyloid beta-peptide and other oxidative stressors: relevance to Alzheimer's disease and other oxidative stress-related neurodegenerative disorders. *Free Radical Biol. Med. 41*, 1694−1703.
(38) Goggel, R., Winoto-Morbach, S., Vielhaber, G., Imai, Y., Lindner, K., Brade, L., Brade, H., Ehlers, S., Slutsky, A. S., Schutze, S., Gulbins, E., and Uhlig, S. (2004) PAF-mediated pulmonary edema: a new role for acid sphingomyelinase and ceramide. *Nat. Med. 10*, 155−160.
(39) Zhou, M., Diwu, Z., Panchuk-Voloshina, N., and Haugland, R. P. (1997) A stable nonfluorescent derivative of resorufin for the fluorometric determination of trace hydrogen peroxide: applications in detecting the activity of phagocyte NADPH oxidase and other oxidases. *Anal. Biochem. 253*, 162−168.
(40) Amtmann, E. (1996) The antiviral, antitumoural xanthate D609 is a competitive inhibitor of phosphatidylcholine-specific phospholipase C. *Drugs Exp. Clin. Res. 22*, 287−294.
(41) Thuren, T., Virtanen, J. A., Somerharju, P. J., and Kinnunen, P. K. (1988) Phospholipase A2 assay using an intramolecularly quenched pyrene-labeled phospholipid analog as a substrate. *Anal. Biochem. 170*, 248−255.
(42) Hendrickson, H. S., Hendrickson, E. K., Johnson, I. D., and Farber, S. A. (1999) Intramolecularly quenched BODIPY-labeled phospholipid analogs in phospholipase A(2) and platelet-activating factor acetylhydrolase assays and in vivo fluorescence imaging. *Anal. Biochem. 276*, 27−35.
(43) Wichmann, O., Gelb, M. H., and Schultz, C. (2007) Probing phospholipase a(2) with fluorescent phospholipid substrates. *ChemBioChem 8*, 1555−1569.
(44) Farber, S. A., Olson, E. S., Clark, J. D., and Halpern, M. E. (1999) Characterization of Ca2+-dependent phospholipase A2 activity during zebrafish embryogenesis. *J. Biol. Chem. 274*, 19338−19346.
(45) Prestwich, G. D., Chen, R., Feng, L., Ozaki, S., Ferguson, C. G., Drees, B. E., Neklason, D. A., Mostert, M. J., Porter-Gill, P. A., Kang, V. H., Shope, J. C., Neilsen, P. O., and Dewald, D. B. (2002) In situ detection of phospholipid and phosphoinositide metabolism. *Adv. Enzyme Regul. 42*, 19−38.
(46) Manna, D., and Cho, W. (2007) In *Methods in Enzymology* (Brown, H. A., Ed.) pp 15−28, Academic Press, New York.
(47) Rose, T. M., and Prestwich, G. D. (2006) Synthesis and evaluation of fluorogenic substrates for phospholipase D and phospholipase C. *Org. Lett. 8*, 2575−2578.
(48) Frangioni, J. V. (2003) In vivo near-infrared fluorescence imaging. *Curr. Opin. Chem. Biol. 7*, 626−634.
(49) Caramelo, J. J., Florin-Christensen, J., Florin-Christensen, M., and Delfino, J. M. (2000) Mapping the catalytic pocket of phospholipases A2 and C using a novel set of phosphatidylcholines. *Biochem. J. 346* (Pt 3), 679−690.
(50) el-Sayed, M. Y., DeBose, C. D., Coury, L. A., and Roberts, M. F. (1985) Sensitivity of phospholipase C (*Bacillus cereus*) activity to phosphatidylcholine structural modifications. *Biochim. Biophys. Acta 837*, 325−335.
(51) Lewis, K. A., Bian, J. R., Sweeney, A., and Roberts, M. F. (1990) Asymmetric short-chain phosphatidylcholines: defining chain binding constraints in phospholipases. *Biochemistry 29*, 9962−9970.
(52) Wolf, R. A., and Gross, R. W. (1985) Identification of neutral active phospholipase C which hydrolyzes choline glycerophospholipids and plasmalogen selective phospholipase A2 in canine myocardium. *J. Biol. Chem. 260*, 7295−7303.
(53) Clark, M. A., Shorr, R. G., and Bomalaski, J. S. (1986) Antibodies prepared to *Bacillus cereus* phospholipase C crossreact with a phosphatidylcholine preferring phospholipase C in mammalian cells. *Biochem. Biophys. Res. Commun. 140*, 114−119.
(54) Spadaro, F., Ramoni, C., Mezzanzanica, D., Miotti, S., Alberti, P., Cecchetti, S., Iorio, E., Dolo, V., Canevari, S., and Podo, F. (2008) Phosphatidylcholine-specific phospholipase C activation in epithelial ovarian cancer cells. *Cancer Res. 68*, 6541−6549.
(55) Kircher, M. F., Josephson, L., and Weissleder, R. (2002) Ratio imaging of enzyme activity using dual wavelength optical reporters. *Mol. Imaging 1*, 89−95.
(56) Bogdanov, A. A. Jr., Lin, C. P., Simonova, M., Matuszewski, L., and Weissleder, R. (2002) Cellular activation of the self-quenched fluorescent reporter probe in tumor microenvironment. *Neoplasia 4*, 228−236.
(57) Messerli, S. M., Prabhakar, S., Tang, Y., Shah, K., Cortes, M. L., Murthy, V., Weissleder, R., Breakefield, X. O., and Tung, C. H. (2004) A novel method for imaging apoptosis using a caspase-1 near-infrared fluorescent probe. *Neoplasia 6*, 95−105.